Wheel Velocity Obstacles for Differential Drive Robot Navigation

Jae D. Jeon and Beom H. Lee
Department of Electrical and Computer Engineering, Seoul National University, Seoul, the Republic of Korea
Email: {innocent88, bhlee}@snu.ac.kr

***Abstract*—In this paper, we deal with the real-time navigation problem of a differential drive robot in dynamic environments. As a rule, the robot is controlled by wheel velocity commands at sampling intervals and moves along a straight line or a circular arc in accordance with those commands. Thus, we define the wheel velocity obstacle, which is a set of all the left and right wheel velocity pairs that induce collisions with obstacles within a given time horizon. Also, a navigation strategy is suggested that will allow the robot to reach its destination without colliding with obstacles. Our algorithm was found to outperform previously released collision avoidance algorithms in terms of safety through Monte Carlo simulations.**

***Index Terms*—collision avoidance, motion planning, velocity obstacles, differential drive robot**

I. Introduction

This paper addresses the local navigation of a mobile robot in dynamic environments, which is one of the most fundamental problems in robotics. The robot with range sensors scans the vicinity and detects nearby obstacles to decide its movement in performing given tasks while avoiding obstacles. Because the sensor inputs are updated periodically, the robot is controlled in discrete time. The representative studies on the local navigation are the potential field approach [1], vector field histogram [2], and velocity obstacle approach [3].

Additionally, we deal with a differential drive robot with non-holonomic kinematic constraints. Heretofore efforts to solve the non-holonomic robot navigation problem have generally followed these two steps: first, the robot's trajectory is generated based on the *supposition* that the robot is holonomic; second, the robot tracks the trajectory closely by using the controller with non-holonomic constraints. However, the supposition in the first step makes a tracking error between the ideal holonomic trajectory and the real trajectory inevitable, as mentioned in [4] and shown in Fig. 1. This difference causes the robot's collision with obstacles no matter how well the robot's trajectory is planned.

To remedy this problem, some studies considered non-holonomic constraints directly. The dynamic window approach in [5] reflected not only the constraints but also the robot dynamics. A dipolar potential function was suggested by [6] to make two non-holonomic mobile robots handling a deformable object avoid collisions in an environment. These two methods was limited in that they could be applied to only static environments.

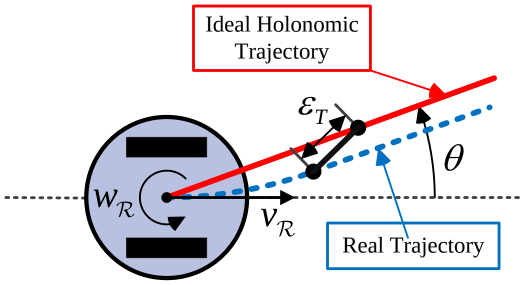

Figure 1. Tracking error ε_T between the ideal holonomic trajectory and the real trajectory. The robot moves in the θ direction.

On the contrary, [7] and [8] took dynamic obstacles into consideration. They defined Dynamic Velocity Space (DVS) that contained the potential collision information, which is the robot's velocity and the corresponding collision time, and utilized the space to find the optimal command. In addition, [9] generalized the velocity obstacle [3] to deal with the constraints of a car-like robot by calculating the minimum distance between the robot and obstacle for randomly sampled controls. Reference [10] applied the concept of the velocity obstacle to the DVS for reducing computational complexity. However, [10] suffered in finding the relevant velocity for the next sampling period due to a disagreement in the linear and angular velocity units.

This paper extends the results of [10] to solve the aforementioned problem. The wheel velocity obstacle (WVO) is defined as a set of wheel velocity pairs that induce collisions within the predefined time horizon and utilized for the robot's local navigation. Since the wheel velocity units are identical, the problem in [10] can be solved.

The rest of this paper is organized as follows: We define the local navigation problem of a differential drive robot and provide some preliminary information in Section II. In Section III, we formalize the concept of the WVO and mathematically derive it before using it to navigate the robot among multiple obstacles in Section IV. In Section V, we present the simulation results and compare them with prior studies. Finally, a conclusion is provided in Section VI.

Manuscript received July 10, 2014; revised october 11, 2014.

doi: 10.12720/joace.3.5.347-353

II. Preliminaries

A. Problem Definition

A differential drive robot, $\mathcal{R}$, navigates to a destination in a two-dimensional plane while avoiding collisions with obstacles. The world inertial frame and the frame attached to $\mathcal{R}$ are denoted by $\mathcal{F}_{\mathcal{W}} = \{O_{\mathcal{W}}, X_{\mathcal{W}}, Y_{\mathcal{W}}\}$ and $\mathcal{F}_{\mathcal{R}} = \{O_{\mathcal{R}}, X_{\mathcal{R}}, Y_{\mathcal{R}}\}$ respectively, as shown in Fig. 2.

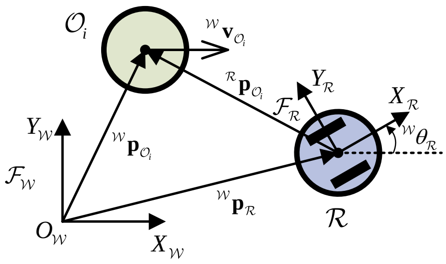

Figure 2. The world inertial frame $\mathcal{F}_{\mathcal{W}}$ and the frame $\mathcal{F}_{\mathcal{R}}$ attached to the robot $\mathcal{R}$.

The robot is circular with radius $r_{\mathcal{R}}$. It is currently located at ${}^{\mathcal{W}}\mathbf{p}_{\mathcal{R}}$ and facing ${}^{\mathcal{W}}\theta_{\mathcal{R}}$ direction with respect to $\mathcal{F}_{\mathcal{W}}$. The robot has two drive wheels mounted on a common axis, each of which is operated independently. The distance between the wheels is l, and the left and right wheel velocities along the ground are $v_{\mathcal{R},L}$ and $v_{\mathcal{R},R}$. Furthermore, they are limited by the maximum wheel velocity, $v_{\mathcal{R}}^{\max}$, and the maximum wheel acceleration, $a_{\mathcal{R}}^{\max}$. In addition to $\mathcal{R}$, there are n obstacles in the workspace. A set of obstacles is referred to as $\mathcal{O}$, and each obstacle $\mathcal{O}_i \in \mathcal{O}$ is circular with radius $r_{\mathcal{O}_i}$. It is currently located at ${}^{\mathcal{W}}\mathbf{p}_{\mathcal{O}_i}$ and moves with velocity ${}^{\mathcal{W}}\mathbf{v}_{\mathcal{O}_i}$.

The robot employs a discrete-time control strategy with constant sampling time Δt and is moved by the wheel velocity commands. At each time instant t_k, it observes the position and velocity of the obstacles that falls in the detection region expressed as

$$D(t_k) = \left\{ \mathbf{x} \in \mathbb{R}^2 \,\middle|\, \left\| \mathbf{x} - {}^{\mathcal{W}}\mathbf{p}_{\mathcal{R}}(t_k) \right\|_2 \le \rho_d \right\} \tag{1}$$

where ρ_d is the radius of the region. The set of obstacles in region D is $\mathcal{DS}$, which helps $\mathcal{R}$ compute its new wheel velocities, $v_{\mathcal{R},L}^{\text{new}}$ and $v_{\mathcal{R},R}^{\text{new}}$, in the next sampling interval so that the robot reach the destination, ${}^{\mathcal{W}}\mathbf{p}_{\mathcal{R}}^{\text{goal}}$, while avoiding the obstacles. The new velocities have to satisfy the velocity and acceleration constraints and be as close to the preferred wheel velocities, $v_{\mathcal{R},L}^{\text{pref}}$ and $v_{\mathcal{R},R}^{\text{pref}}$, as possible.

B. Differential Drive Robot Kinematics

A differential drive robot is operated by the rotary motion of its two wheels. As a result, the robot cannot move in the lateral direction:

$$\left(\frac{d}{dt} {}^{\mathcal{W}}\mathbf{p}_{\mathcal{R}} \right)^T \mathbf{R}(90°)\mathbf{u}\left({}^{\mathcal{W}}\theta_{\mathcal{R}} \right) = 0 \tag{2}$$

where $\mathbf{R}(\theta) \in \mathrm{SO}(2)$ is the planar rotation matrix corresponding to angle θ and $\mathbf{u}(\theta) = [\cos\theta \quad \sin\theta]^T$ is the unit vector with direction θ. Therefore, the motion of the robot is characterized by its linear and angular velocities $v_{\mathcal{R}}$ and $w_{\mathcal{R}}$, where

$$v_{\mathcal{R}} = \frac{v_{\mathcal{R},L} + v_{\mathcal{R},R}}{2}, \; w_{\mathcal{R}} = \frac{v_{\mathcal{R},R} - v_{\mathcal{R},L}}{l} \tag{3}$$

Suppose the robot maintains its velocities for a sampling time, Δt. Then it moves along the circular arc with signed radius and center of r_c and ${}^{\mathcal{W}}\mathbf{p}_c$, respectively.

$$r_c = \frac{l}{2} \frac{v_{\mathcal{R},L} + v_{\mathcal{R},R}}{v_{\mathcal{R},R} - v_{\mathcal{R},L}} \tag{4}$$

$${}^{\mathcal{W}}\mathbf{p}_c = {}^{\mathcal{W}}\mathbf{p}_{\mathcal{R}} - r_c \mathbf{R}(90°)\mathbf{u}\left({}^{\mathcal{W}}\theta_{\mathcal{R}} \right) \tag{5}$$

At the next time instant t_{k+1}, the robot's position and heading direction are

$${}^{\mathcal{W}}\mathbf{p}_{\mathcal{R}}(t_{k+1}) = {}^{\mathcal{W}}\mathbf{p}_c + \mathbf{R}(w_{\mathcal{R}}\Delta t)\left({}^{\mathcal{W}}\mathbf{p}_{\mathcal{R}}(t_k) - {}^{\mathcal{W}}\mathbf{p}_c \right) \tag{6}$$

$${}^{\mathcal{W}}\theta_{\mathcal{R}}(t_{k+1}) = {}^{\mathcal{W}}\theta_{\mathcal{R}}(t_k) + w_{\mathcal{R}}\Delta t \tag{7}$$

The radius in (4), however, diverges to infinity when the left and right wheel velocities are equivalent. In other words, the robot moves along a straight line. Therefore, the robot's position at the next time instant is changed to but the heading direction is invariant.

$${}^{\mathcal{W}}\mathbf{p}_{\mathcal{R}}(t_k + \Delta t) = {}^{\mathcal{W}}\mathbf{p}_{\mathcal{R}}(t_k) + v_{\mathcal{R}}\Delta t \cdot \mathbf{u}\left({}^{\mathcal{W}}\theta_{\mathcal{R}} \right) \tag{8}$$

C. Mapping Obstacles to the Configuration Space

When planning the differential drive robot's motion, it is more intuitive to consider obstacles in the configuration space. In the process of mapping them from the workspace to the configuration space, the radius of obstacle $\mathcal{O}_i$ increases from $r_{\mathcal{O}_i}$ to $r_{\mathcal{O}_i} + r_{\mathcal{R}}$. The position and velocity of the obstacle $\mathcal{O}_i$ are

$${}^{\mathcal{R}}\mathbf{p}_{\mathcal{O}_i} = \mathbf{R}\left(-{}^{\mathcal{W}}\theta_{\mathcal{R}} \right)\left({}^{\mathcal{W}}\mathbf{p}_{\mathcal{O}_i} - {}^{\mathcal{W}}\mathbf{p}_{\mathcal{R}} \right) \tag{9}$$

$${}^{\mathcal{R}}\mathbf{v}_{\mathcal{O}_i} = \mathbf{R}\left(-{}^{\mathcal{W}}\theta_{\mathcal{R}} \right) {}^{\mathcal{W}}\mathbf{v}_{\mathcal{O}_i} \tag{10}$$

viewed with respect to $\mathcal{F}_{\mathcal{R}}$. The obstacle mapped from $\mathcal{O}_i$ is denoted by $\mathcal{QO}_i$ such that

$$\mathcal{QO}_i = \left\{ \mathbf{x} \in \mathbb{R}^2 \,\middle|\, \left\| \mathbf{x} - {}^{\mathcal{R}}\mathbf{p}_{\mathcal{O}_i} \right\|_2 \le r_{\mathcal{O}_i} + r_{\mathcal{R}} \right\} \tag{11}$$

For the sake of simplicity, the pre-superscripts of ${}^{\mathcal{R}}\mathbf{p}_{\mathcal{O}_i}$ and ${}^{\mathcal{R}}\mathbf{v}_{\mathcal{O}_i}$ are discarded to be $\mathbf{p}_{\mathcal{O}_i}$ and $\mathbf{v}_{\mathcal{O}_i}$ hereafter.

III. Wheel Velocity Obstacles

In this section, we describe the WVO so that a differential drive robot navigates to the destination without collisions. We first introduce the concept of the WVO and then elucidate how to construct them.

The wheel velocity obstacle $WVO_{\mathcal{R}|\mathcal{O}_i}^{\tau}$ is defined as the set of all the left-right wheel velocity pairs that would induce a collision with obstacle $\mathcal{O}_i$ within time τ. The robot avoids colliding with $\mathcal{O}_i$ before time $t_k + \tau$ if the new wheel velocity pair $(v_{\mathcal{R},L}^{\text{new}}, v_{\mathcal{R},R}^{\text{new}})$ does not belong to $WVO_{\mathcal{R}|\mathcal{O}_i}^{\tau}$ at time t_k.

In contrast with the original velocity obstacle suggested in [3], the overall shape of the WVO is somewhat complicated due to the nonlinearity of the robot's motion. To derive it, we will divide it into two sets according to the geometry of the robot's path: $SWVO_{\mathcal{R}|\mathcal{O}_i}^{\tau}$ and $CWVO_{\mathcal{R}|\mathcal{O}_i}^{\tau}$ such that $WVO_{\mathcal{R}|\mathcal{O}_i}^{\tau} = SWVO_{\mathcal{R}|\mathcal{O}_i}^{\tau} \bigcup CWVO_{\mathcal{R}|\mathcal{O}_i}^{\tau}$. $SWVO_{\mathcal{R}|\mathcal{O}_i}^{\tau}$ is the WVO when the robot moves along a straight line, and $CWVO_{\mathcal{R}|\mathcal{O}_i}^{\tau}$ is the WVO when it moves along a circular curve. For the latter set, there must be a difference between the static and dynamic obstacle. The following three cases are analyzed accordingly.

A. Straight Line Path

First, we consider the case where the robot's wheel velocities are equivalent. To find the WVO region, we review the concept of original velocity obstacles [3] since the robot and obstacle move along a straight line path. This region is represented as

$$SWVO_{\mathcal{R}|\mathcal{O}_i}^{\tau} = \left\{(v,v) \in \mathbb{R}^2 \middle| \lambda(v) \bigcap \mathcal{QO}_i \neq \varnothing \right\} \tag{12}$$

where $\lambda(\cdot)$ is the line such that

$$\lambda(v) = \left\{ t\left(\begin{bmatrix} v & 0 \end{bmatrix}^T - \mathbf{v}_{\mathcal{O}_i}\right) \middle| 0 \le t \le \tau \right\} \tag{13}$$

here, velocity v is the x-coordinate of a point in the intersection between the original velocity obstacle, $VO_{\mathcal{R}|\mathcal{O}_i}^{\tau}$ in [3], and the x-axis if and only if $(v,v) \in SWVO_{\mathcal{R}|\mathcal{O}_i}^{\tau}$, as shown in Fig. 3.

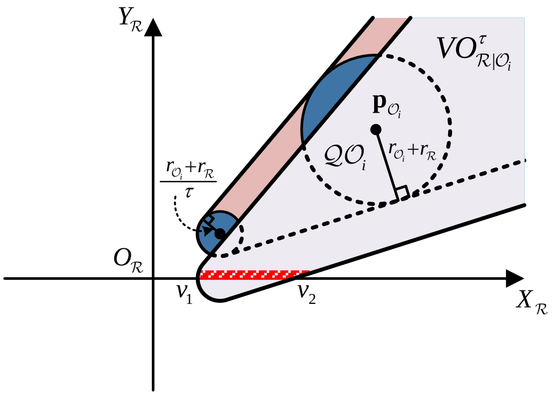

Figure 3. The original velocity obstacle of [3] and the red line on the x-axis. The red line is the range of v that satisfies $\lambda(v) \bigcap \mathcal{QO}_i \neq \varnothing$. Hence, $SWVO_{\mathcal{R}|\mathcal{O}_i}^{\tau} = \{(\mathrm{v},\mathrm{v}) \in \mathbb{R}^2 \mid v_1 < \mathrm{v} < v_2\}$.

B. Circular Curve Path / Static Obstacle

Suppose the robot makes the circular path with radius r_c and avoids a static obstacle, $\mathcal{O}_s$. In the robot's configuration space, the center of the path is at $\mathbf{p}_c = (0, r_c)$. Fig. 4 shows the range of the path's radius that induces a collision between the robot and the obstacle, as well as the angular position at which the collision occurs.

Incidentally, the angular position, φ, is defined according to the robot's wheel velocities. The angular position is measured counterclockwise if $w_{\mathcal{R}} > 0$ and clockwise for all other cases. The zero angular position is defined as the direction from $\mathbf{p}_c$ to the origin.

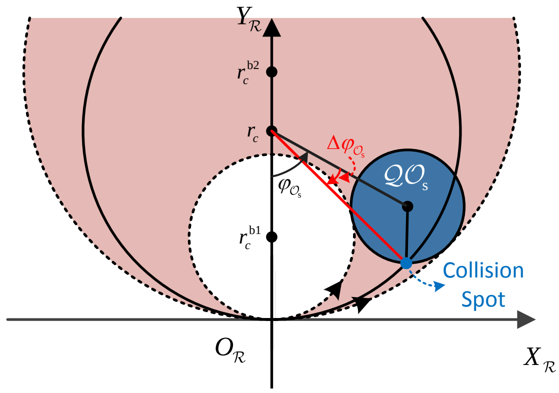

Figure 4. The range of the radius making the robot collide with obstacle $\mathcal{O}_s$, and the collision spot where the collision occurs.

The boundaries of the forbidden radii, r_c^{b}, satisfy the following equation:

$$p_{\mathcal{O}_s,x}^2 + \left(p_{\mathcal{O}_s,y} - r_c^{\mathrm{b}}\right)^2 = \left(r_{\mathcal{O}_s} + r_{\mathcal{R}} \pm r_c^{\mathrm{b}}\right)^2 \tag{14}$$

From (14), we get

$$r_c^{\mathrm{b}} = \frac{p_{\mathcal{O}_s,x}^2 + p_{\mathcal{O}_s,y}^2 - \left(r_{\mathcal{O}_s} + r_{\mathcal{R}}\right)^2}{2\left(p_{\mathcal{O}_s,y} \pm \left(r_{\mathcal{O}_s} + r_{\mathcal{R}}\right)\right)} \tag{15}$$

Let r_c^{b1} and r_c^{b2} denote the values of (15) such that $r_c^{\mathrm{b1}} \le r_c^{\mathrm{b2}}$. If the robot moves along a circular arc with radius r_c where

$$r_c^{\mathrm{b1}} r_c^{\mathrm{b2}} \left(r_c - r_c^{\mathrm{b1}}\right)\left(r_c - r_c^{\mathrm{b2}}\right) < 0 \tag{16}$$

It will meet $\mathcal{O}_s$ at some time in the future.

We are interested in whether the collision is generated within time τ when the radius satisfy (16). The collision time must be calculated in accordance with the robot's velocities. We first compute the angular position of the collision spot. When the robot's wheel velocity pair $(v_{\mathcal{R},L}, v_{\mathcal{R},R})$ is given, $\varphi_{\mathcal{O}_s}$ denotes the angular position of the center of $\mathcal{O}_s$ such that

$$\varphi_{\mathcal{O}_s} = \operatorname{sgn}\left(w_{\mathcal{R}}\right) \cdot \angle\left(\mathbf{p}_{\mathcal{O}_s} - \mathbf{p}_c\right) + \operatorname{sgn}\left(v_{\mathcal{R}}\right) \cdot \frac{\pi}{2} \tag{17}$$

where $\angle(\mathbf{v})$ represents the angle of vector $\mathbf{v}$ to coordinate axes, and $v_{\mathcal{R}}$ and $w_{\mathcal{R}}$ are calculated from (3). $\Delta\varphi_{\mathcal{O}_s}$ is given by the angular difference between the center of $\mathcal{O}_s$ and the collision spot with respect to $\mathbf{p}_c$. Using the second law of cosines,

$$\Delta\varphi_{\mathcal{O}_s} = \arccos \frac{p_{\mathcal{O}_s,x}^2 + \left(p_{\mathcal{O}_s,y} - r_c\right)^2 + r_c^2 - \left(r_{\mathcal{O}_s} + r_{\mathcal{R}}\right)^2}{2 r_c \sqrt{p_{\mathcal{O}_s,x}^2 + \left(p_{\mathcal{O}_s,y} - r_c\right)^2}} \tag{18}$$

where r_c is from (4), and the angular displacement of the collision spot is calculated by $\varphi_{\mathcal{O}_s} - \Delta\varphi_{\mathcal{O}_s}$ from (17) and

(18). Hence, the wheel velocity obstacle $CWVO^{\tau}_{\mathcal{R}|\mathcal{O}_s}$ is now defined as

$$CWVO^{\tau}_{\mathcal{R}|\mathcal{O}_s} = \{(v_{\mathcal{R},L}, v_{\mathcal{R},R}) \in \mathbb{R}^2 | v_{\mathcal{R},R} \neq v_{\mathcal{R},L} \\ l(\varphi_{\mathcal{O}_s} - \Delta\varphi_{\mathcal{O}_s}) \leq \tau |v_{\mathcal{R},R} - v_{\mathcal{R},L}|\} \tag{19}$$

C. Circular Curve Path / Dynamic Obstacle

In this subsection, we extend the results of [7] and [10]. In [7], the Collision Band is defined as the zone swept by the object moving along a straight line. Let $\mathbf{a}_{\mathcal{O}_d}$ denote a vector that is perpendicular to the heading direction of $\mathcal{O}_d$ and is directed against the origin such that

$$\mathbf{a}_{\mathcal{O}_d} = \operatorname{sgn}\left(\mathbf{p}^T_{\mathcal{O}_d}\mathbf{R}(90°)\mathbf{v}_{\mathcal{O}_d}\right)\mathbf{R}(90°)\mathbf{v}_{\mathcal{O}_d} / \|\mathbf{v}_{\mathcal{O}_d}\|_2 \tag{20}$$

where $\operatorname{sgn}(\cdot)$ is the modified sign function such that $\operatorname{sgn}(0)=1$. Also, $\mathbf{b}_{\mathcal{O}_d,i}$, $i=1,2$ refer to the contact points between $\mathcal{O}_d$ and the boundaries of the Collision Band such that $\mathbf{b}_{\mathcal{O}_d,1}$ is on the boundary closer to the origin and $\mathbf{b}_{\mathcal{O}_d,2}$ is on the other line. Thus, the two points are expressed as

$$\mathbf{b}_{\mathcal{O}_d,1} = \mathbf{p}_{\mathcal{O}_d} - (r_{\mathcal{O}_d} + r_{\mathcal{R}})\mathbf{a}_{\mathcal{O}_d} \tag{21}$$

$$\mathbf{b}_{\mathcal{O}_d,2} = \mathbf{p}_{\mathcal{O}_d} + (r_{\mathcal{O}_d} + r_{\mathcal{R}})\mathbf{a}_{\mathcal{O}_d} \tag{22}$$

Fig. 5 presents two red arcs, A_1 and A_2, that shows the intersection of the robot's path and the Collision Band. Let $\mathcal{A}$ be a set of these arcs. The robot and the obstacle do not meet each other in A_i, $i=1$ or 2 if the robot enters A_i when the obstacle has just excited it or if the robot escapes from A_i when the obstacle is entering it, as mentioned in [7]. For this reason, we need to know when the obstacle overlaps with A_i and where the robot enters or exits from A_i. We will derive the wheel velocity obstacle based on whether the robot is located in the Collision Band or not

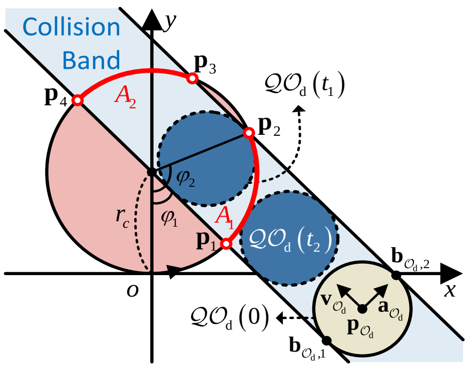

Figure 5. The robot's path and the collision band of the obstacle. The red arcs are the intersection between them. No collision occurs if the robot arrives at $\mathbf{p}_1$ after time t_1 or leaves from $\mathbf{p}_2$ before time t_2.

If the Collision Band does not include the origin, the number of the intersection arcs, $\mathcal{N}(\mathcal{A})$, varies depending on the radius of the path.

$$\mathcal{N}(\mathcal{A}) = \begin{cases} 0, & |r_c| + \mathbf{p}_c^T\mathbf{a}_{\mathcal{O}_d} \leq \mathbf{b}^T_{\mathcal{O}_d,1}\mathbf{a}_{\mathcal{O}_d}, \\ 1, & \mathbf{b}^T_{\mathcal{O}_d,1}\mathbf{a}_{\mathcal{O}_d} < |r_c| + \mathbf{p}_c^T\mathbf{a}_{\mathcal{O}_d} \leq \mathbf{b}^T_{\mathcal{O}_d,2}\mathbf{a}_{\mathcal{O}_d}. \\ 2, & \text{otherwise.} \end{cases} \tag{23}$$

We divide $CWVO^{\tau}_{\mathcal{R}|\mathcal{O}_d}$ into $CWVO^{\tau}_{\mathcal{R}|\mathcal{O}_d,i}$, $i=1,2$ on the basis of the number of the arcs where index i represents $\mathcal{N}(\mathcal{A})$. We define the set $\mathcal{V}_i \subset \mathbb{R}^2$ such that $(v_{\mathcal{R},L}, v_{\mathcal{R},R}) \in \mathcal{V}_i$ if and only if $\mathcal{N}(\mathcal{A}) = i$ when the robot moves with that velocity.

If $\mathcal{N}(\mathcal{A}) = 1$, the obstacle meets $\mathcal{A}$ from t_1 to t_2. The times t_1 and t_2 are calculated by $t_1 = t_{\text{center}} - t_{\text{offset1}}$ and $t_2 = t_{\text{center}} + t_{\text{offset1}}$ where

$$t_{\text{center}} = (\mathbf{p}_c - \mathbf{p}_{\mathcal{O}_d})^T \mathbf{v}_{\mathcal{O}_d} / \|\mathbf{v}_{\mathcal{O}_d}\|_2^2 \tag{24}$$

$$t_{\text{offset1}} = \frac{\sqrt{(|r_c| + r_{\mathcal{O}_d} + r_{\mathcal{R}})^2 - ((\mathbf{p}_c - \mathbf{p}_{\mathcal{O}_d})^T \mathbf{a}_{\mathcal{O}_d})^2}}{\|\mathbf{v}_{\mathcal{O}_d}\|_2} \tag{25}$$

In order to find the angular positions φ_1 and φ_2 where the robot enters or exits from the intersection, φ_{offset1} must be defined.

$$\varphi_{\text{offset1}} = \arccos\left((\mathbf{b}_{\mathcal{O}_d,1} - \mathbf{p}_c)^T \mathbf{a}_{\mathcal{O}_d} / |r_c|\right) \tag{26}$$

Then $\varphi_1 = \Delta\varphi_{\mathcal{O}_d} - \varphi_{\text{offset1}}$ and $\varphi_2 = \Delta\varphi_{\mathcal{O}_d} + \varphi_{\text{offset1}}$ where $\Delta\varphi_{\mathcal{O}_d}$ is from (18). Thus, the wheel velocity obstacle is expressed as

$$CWVO^{\tau}_{\mathcal{R}|\mathcal{O}_d,1} = \Big\{(v_{\mathcal{R},L}, v_{\mathcal{R},R}) \in \mathcal{V}_1 \Big| t_1 < \tau, t_2 > 0, k \in \mathbb{N}_0 \\ \frac{l(\varphi_1 + 2\pi k)}{\min\{t_2, \tau\}} < |v_{\mathcal{R},R} - v_{\mathcal{R},L}| < \frac{l(\varphi_2 + 2\pi k)}{\max\{t_1, 0\}}\Big\} \tag{27}$$

Here, the constraints that contain 0 and τ such as $t_1 < \tau$ are inserted for the collision generated within time τ. Since the motion of the robot along the circular path is periodic, the terms of $2\pi k$ are added.

If $\mathcal{N}(\mathcal{A}) = 2$, put $t_1 = t_{\text{center}} - t_{\text{offset1}}$, $t_2 = t_{\text{center}} - t_{\text{offset2}}$, $t_3 = t_{\text{center}} + t_{\text{offset2}}$, and $t_4 = t_{\text{center}} + t_{\text{offset1}}$

where

$$t_{\text{offset2}} = \frac{\sqrt{(|r_c| - (r_{\mathcal{O}_d} + r_{\mathcal{R}}))^2 - ((\mathbf{p}_c - \mathbf{p}_{\mathcal{O}_d})^T \mathbf{a}_{\mathcal{O}_d})^2}}{\|\mathbf{v}_{\mathcal{O}_d}\|_2} \tag{28}$$

The obstacle overlaps with the intersection arcs after $t \in (t_1, t_2)$ or $t \in (t_3, t_4)$.

Likewise, put $\varphi_1 = \Delta\varphi_{\mathcal{O}_d} - \varphi_{\text{offset1}}$, $\varphi_2 = \Delta\varphi_{\mathcal{O}_d} - \varphi_{\text{offset2}}$, $\varphi_3 = \Delta\varphi_{\mathcal{O}_d} + \varphi_{\text{offset2}}$, and $\varphi_4 = \Delta\varphi_{\mathcal{O}_d} + \varphi_{\text{offset1}}$ where

$$\varphi_{\text{offset2}} = \arccos\left((\mathbf{b}_{\mathcal{O}_d,2} - \mathbf{p}_c)^T \mathbf{a}_{\mathcal{O}_d} / |r_c|\right) \tag{29}$$

The robot is in the Collision band when its angular position along the path is in the intersection (φ_1, φ_2) or (φ_3, φ_4).

To derive the wheel velocity obstacle, each of the angular position segments must be associated with the relevant time segment. If $\operatorname{sgn}(w_{\mathcal{R}}) \cdot \mathbf{a}^T_{\mathcal{O}_d}\mathbf{R}(90°)\mathbf{v}_{\mathcal{O}_d} > 0$, the obstacle moves counterclockwise with respect to the origin in the robot's configuration space. We define the function $\gamma : \mathcal{I} \to \mathcal{I}$ where $\mathcal{I} = \{1, 2, 3, 4\}$ such that $\gamma(x) = x$. If it does not, then the function γ is defined as $\gamma(x) = \mathrm{mod}(x+1, 4)+1$. Thus, the wheel velocity obstacle is expressed as

$$\begin{aligned} CWVO^{\tau}_{\mathcal{R}|\mathcal{O}_d,2} = &\Big\{ (v_{\mathcal{R},L}, v_{\mathcal{R},R}) \in \mathcal{V}_2 \Big| t_1 < \tau, t_2 > 0, k \in \mathbb{N}_0, \\ &\frac{l(\varphi_{\gamma(1)} + 2\pi k)}{\min\{t_2, \tau\}} < |v_{\mathcal{R},R} - v_{\mathcal{R},L}| < \frac{l(\varphi_{\gamma(2)} + 2\pi k)}{\max\{t_1, 0\}} \Big\} \\ &\cup \Big\{ (v_{\mathcal{R},L}, v_{\mathcal{R},L}) \in \mathcal{V}_2 \Big| t_3 < \tau, t_4 > 0, k \in \mathbb{N}_0, \\ &\frac{l(\varphi_{\gamma(3)} + 2\pi k)}{\min\{t_4, \tau\}} < |v_{\mathcal{R},R} - v_{\mathcal{R},L}| < \frac{l(\varphi_{\gamma(4)} + 2\pi k)}{\max\{t_3, 0\}} \Big\}. \end{aligned} \tag{30}$$

In the case when the collision band includes the origin,

$$\mathcal{N}(\mathcal{A}) = \begin{cases} 0, & |r_c| \le \min\{\mathbf{p}_c^T \mathbf{a}_{\mathcal{O}_d} - \mathbf{b}^T_{\mathcal{O}_d,1}\mathbf{a}_{\mathcal{O}_d}, \\ & \qquad -\mathbf{p}_c^T \mathbf{a}_{\mathcal{O}_d} + \mathbf{b}^T_{\mathcal{O}_d,2}\mathbf{a}_{\mathcal{O}_d}\} \\ 1, & (|r_c| - \mathbf{p}_c^T \mathbf{a}_{\mathcal{O}_d} + \mathbf{b}^T_{\mathcal{O}_d,1}\mathbf{a}_{\mathcal{O}_d}) \\ & \quad \cdot (|r_c| + \mathbf{p}_c^T \mathbf{a}_{\mathcal{O}_d} + \mathbf{b}^T_{\mathcal{O}_d,2}\mathbf{a}_{\mathcal{O}_d}) \le 0, \\ 2, & \text{otherwise.} \end{cases} \tag{31}$$

When $\mathcal{N}(\mathcal{A}) = 0$, the circle, not an arc, intersects with the Collision Band. Therefore, the robot cannot escape from the band. As a result, the wheel velocity obstacle is

$$CWVO^{\tau}_{\mathcal{R}|\mathcal{O}_d,0} = \Big\{ (v_{\mathcal{R},L}, v_{\mathcal{R},R}) \in \mathcal{V}_0 \Big| t_1 < \tau, t_2 > 0 \Big\} \tag{32}$$

Suppose that $\mathcal{N}(\mathcal{A}) = 1$. We calculate φ_{offset1} by substituting $\mathbf{a}_{\mathcal{O}_d}$ of (26) with $-\mathbf{a}_{\mathcal{O}_d}$ if $|r_c| \le \mathbf{p}_c^T \mathbf{a}_{\mathcal{O}_d} - \mathbf{b}^T_{\mathcal{O}_d,1}\mathbf{a}_{\mathcal{O}_d}$ or by substituting $\mathbf{b}_{\mathcal{O}_d,1}$ with $\mathbf{b}_{\mathcal{O}_d,2}$ otherwise. Then put $\varphi_1 = \Delta\varphi_{\mathcal{O}_d} - \varphi_{\text{offset1}}$ and $\varphi_2 = \Delta\varphi_{\mathcal{O}_d} + \varphi_{\text{offset1}}$. Afterward, φ_1 and φ_2 are adjusted to be $\varphi_1 \in [-2\pi, 0)$ and $\varphi_2 \in [0, 2\pi)$, respectively. Finally, the wheel velocity obstacle $CWVO^{\tau}_{\mathcal{R}|\mathcal{O}_d,1}$ is given by (27).

If $\mathcal{N}(\mathcal{A}) = 2$, the condition that the function γ is the identity function is changed to $r_c \cdot v_{\mathcal{O}_d,y} < 0$. $\mathbf{a}_{\mathcal{O}_d}$ of (26) is substituted with $-\mathbf{a}_{\mathcal{O}_d}$. Then we calculate φ_i, $i = 1, \ldots, 4$ and adjust them to be $\varphi_i \in [0, 2\pi)$. The subscript of φ_i is rearranged so that $\varphi_2 \le \varphi_3 \le \varphi_4 \le \varphi_1$, and φ_1 is in the range of $[-2\pi, 0)$. Finally, the wheel velocity obstacle $CWVO^{\tau}_{\mathcal{R}|\mathcal{O}_d,2}$ is obtained by (30).

IV. Navigation among Multiple Obstacles

In this section, we explain how the robot navigates among the multiple obstacles to arrive at the destination without collision.

We first define the observable wheel velocity obstacle such that $WVO^{\tau}_{\mathcal{R}|\mathcal{DO}} = \bigcup_{\mathcal{O}_i \in \mathcal{DO}} WVO^{\tau}_{\mathcal{R}|\mathcal{O}_i}$.

The set of the wheel velocity pairs that the robot can reach in time Δt is denoted by RV_R. From the velocity and acceleration constraints of the robot, RV_R is represented by

$$\begin{aligned} RV_R = &\Big\{ (v^{\text{new}}_{\mathcal{R},L}, v^{\text{new}}_{\mathcal{R},R}) \in \mathbb{R}^2 \Big| -v^{\max}_{\mathcal{R}} \le v^{\text{new}}_{\mathcal{R},L}, v^{\text{new}}_{\mathcal{R},R} \le v^{\max}_{\mathcal{R}} \Big\} \\ &\cap \Big\{ (v^{\text{new}}_{\mathcal{R},L}, v^{\text{new}}_{\mathcal{R},R}) \in \mathbb{R}^2 \Big| |v^{\text{new}}_{\mathcal{R},j} - v_{\mathcal{R},j}| \le a^{\max}_{\mathcal{R}} \Delta t, \ j \in \{L, R\} \Big\} \end{aligned} \tag{33}$$

In addition, the reachable avoidance velocities is denoted by RAV_R such that $RAV_R = RV_R \setminus WVO^{\tau}_{\mathcal{R}|\mathcal{DO}}$. If the robot selects its new velocities in RAV_R, there are no collision until time τ has passed.

The robot's preferred wheel velocities are determined after its preferred linear and angular velocities are calculated. The preferred angular velocity is

$$w^{\text{pref}}_{\mathcal{R}} = 2\angle \mathbf{p}^{\text{goal}}_{\mathcal{R}} \Big/ \left(\delta\left(\|\mathbf{p}^{\text{goal}}_{\mathcal{R}}\| \right) \cdot \Delta t \right) \tag{34}$$

where $\delta(\cdot)$ is a non-decreasing function whose minimum value is 1. In particular, when the destination is close enough for the robot to arrive at the next time, δ gets the minimum value. The preferred linear velocity is

$$v^{\text{pref}}_{\mathcal{R}} = \min\left\{ d^{\text{goal}}_{\mathcal{R}} / \Delta t, v^{\lim}_{\mathcal{R}}\left(w^{\text{pref}}_{\mathcal{R}}\right) \right\} \tag{35}$$

where $v^{\lim}_{\mathcal{R}}(w) = v^{\max}_{\mathcal{R}} - l/2 \cdot |w^{\text{pref}}_{\mathcal{R}}|$, and $d^{\text{goal}}_{\mathcal{R}}$ is the distance between the robot and the destination such that

$$d^{\text{goal}}_{\mathcal{R}} = \begin{cases} p^{\text{goal}}_{\mathcal{R},x}, & \text{if } p^{\text{goal}}_{\mathcal{R},y} = 0, \\ \|\mathbf{p}^{\text{goal}}_{\mathcal{R}}\|_2 \angle \mathbf{p}^{\text{goal}}_{\mathcal{R}} / \sin\left(\angle \mathbf{p}^{\text{goal}}_{\mathcal{R}}\right), & \text{otherwise.} \end{cases} \tag{36}$$

The preferred wheel velocities, $v^{\text{pref}}_{\mathcal{R},L}$ and $v^{\text{pref}}_{\mathcal{R},R}$ are computed by using (3).

If $(v^{\text{pref}}_{\mathcal{R},L}, v^{\text{pref}}_{\mathcal{R},R}) \in RAV_R$, the robot selects $(v^{\text{pref}}_{\mathcal{R},L}, v^{\text{pref}}_{\mathcal{R},R})$ as the new wheel velocity pair $(v^{\text{new}}_{\mathcal{R},L}, v^{\text{new}}_{\mathcal{R},R})$. If not, the robot should find the pair closest to $(v^{\text{pref}}_{\mathcal{R},L}, v^{\text{pref}}_{\mathcal{R},R})$ in RAV_R. Since the geometry of RAV_R is complicated, we adopt a sampling method. First, we randomly sample candidates, $(v^i_L, v^i_R) \in RV_R$, $i = 1, \ldots, N_{\text{sample}}$. Next, the candidates in $WVO^{\tau}_{\mathcal{R}|\mathcal{DO}}$ are eliminated. Finally, the pair closest to $(v^{\text{pref}}_{\mathcal{R},L}, v^{\text{pref}}_{\mathcal{R},R})$ among remaining samples is chosen as $(v^{\text{new}}_{\mathcal{R},L}, v^{\text{new}}_{\mathcal{R},R})$, as described in Fig. 6.

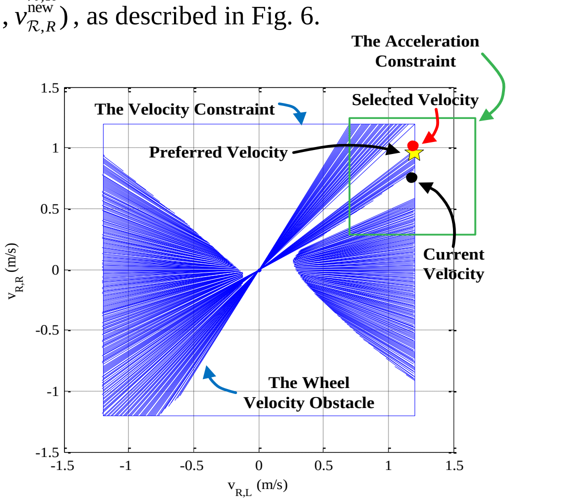

Figure 6. The observable wheel velocity obstacle and the process of selecting a new velocity. The blue square is the velocity constraint, and the green square is the acceleration constraint. The robot's current velocity is indicated by the black mark and its preferred velocity is shown as the yellow star. Because the yellow star is in the wheel velocity obstacle, we choose the red mark as the new velocity,

If $RAV_R = \varnothing$, we remove the farthest obstacle from $\mathcal{OD}$ and redefine the $WVO^{\tau}_{\mathcal{R}|\mathcal{DO}}$ one by one until $RAV_R \neq \varnothing$. At worst, the closest obstacle makes $WVO^{\tau}_{\mathcal{R}|\mathcal{DO}}$ be empty. In this case, we set the time horizon τ as Δt.

V. Simulation

The implementation details are described in the following. The simulation is performed in the Matlab software on a PC equipped with Intel Core i7-3770 3.40GHz CPU and 8GB memory.

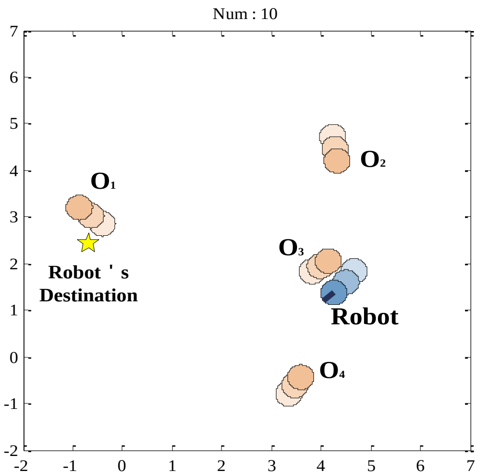

Figure 7. Screenshot of the robot's navigation among 4 obstacles using the wheel velocity obstacles. The number above the image shows the number of trials.

As shown in Fig. 7, the simulation environment is a two-dimensional indoor space of 7m by 7m, where a Pioneer 3DX robot [11] moves toward the destination while avoiding collisions. On the basis of the robot's datasheet, its parameters are assigned. The robot's radius $r_{\mathcal{R}}$ is considered as its swing radius 0.267m, and the distance between the two wheels is 0.381m. In addition, the maximum velocity of the robot is 1.2m/s, and the maximum acceleration is 1.5m/s^2. The maximum detection distance ρ_d is 5m, the sampling period Δt for robot control is 0.3s, and the predefined time horizon τ is 1.5s.

In the simulation space, obstacles move with given random velocities. At each time instant, obstacles change their velocity with probability p_{O_i}. When the robot escapes from the simulation space, its heading direction is switched inwards to the space.

The Monte Carlo simulations are used to demonstrate the performance of the wheel velocity obstacle approach. We simulate the scenario consecutively for easier sample generation. For example, when the robot reaches its destination, the location of the destination is just resampled. When the robot collides with some obstacles in the simulation, the robot is placed in a newly sampled location.

The performance of our algorithm is compared with that of the algorithm [3], which controls a differential robot as if it has no non-holonomic constraint. The total number of scenario samples is 1000. The simulation results are summarized in Table I. Although the average computation time of our algorithm for each sample period is somewhat longer than that in [3], it is not important because the computation time is far shorter than the sampling time. The success rate of the algorithm is much higher than that in [3]. Therefore, it is confirmed that our algorithm outperforms other algorithms in terms of safety.

TABLE I. Simulation Results

Algorithm	Computation time per time step (ms)	Success rate (%)
Proposed	2.2	92.6
[3]	1.9	75.9

VI. Conclusion

In this paper, we derived the wheel velocity obstacle. Since a differential drive robot has nonlinear motion, the derivation process was divided into three cases according to the robot's trajectory and the mobility of obstacles. We suggested a sampling scheme for the robot's local navigation utilizing the wheel velocity obstacle. The proposed algorithm was shown to be superior in avoiding the collisions according to the Monte Carlo simulations.

In future research, we will consider abrupt motion changes of the obstacle since failures in the simulation were induced by the abrupt changes of obstacle's velocity. We will also attempt to avoid collisions between robots.

Acknowledgment

This work was supported in part by the National Research Foundation of Korea (NRF) grant funded by the Korean government (MSIP) (No.2013R1A2A1A0500554 7), the Brain Korea 21 Plus Project, ASRI, the Industrial Foundation Technology Development Program of MOTIE/KEIT (Development of Collective Intelligence Robot Technologies), and the Bio-Mimetic Robot Research Center funded by the Defense Acquisition Program Administration (UD130070ID).

References

[1] S. S. Ge and Y. J. Cui, "Dynamic motion planning for mobile robots using potential field method," *Auton. Robot.*, vol. 13, no. 3, pp. 207-222, Nov. 2002.

[2] Y. Zhu, T. Zhang, J. Song, X. Li, and M. Nakamura, "A new method for mobile robots to avoid collision with moving obstacle," *Artif. Life Robot.*, vol. 16, no. 4, pp. 507-510, Feb. 2012.

[3] P. Fiorini and Z. Shiller, "Motion planning in dynamic environments using velocity obstacles," *Int. J. Robot. Res.*, vol. 17, no. 7, pp. 760-772, July 1998.

[4] J. Alonso-Mora, A. Breitenmoser, M. Rufli, P. Beardsley, and R. Siegwart, "Optimal reciprocal collision avoidance for multiple non-holonomic robots," in *Distributed Autonomous Robotics Systems*, vol. 83 of *Springer Tracts in Advanced Robotics*, A. Martinoli, *et al.* ed. Berlin, Heidelberg: Springer, 2013, pp. 203-216.

[5] D. Fox, W. B. Burgard, and S. Thrun, "The dynamic window approach to collision avoidance," *IEEE Robot. Autom, Mag.*, vol. 4, no. 1, pp. 23-33, Mar. 1997.

[6] H. G. Tanner, S. G. Loizou, and K. J. Kyriakopoulos, “Nonholonomic navigation and control of cooperating mobile manipulators,” *IEEE Trans. Robot. Autom.,* vol. 19, no. 1, pp. 53-64, Feb. 2003.

[7] E. Owen and L. Montano, "Motion planning in dynamic environments using the velocity space," in *Proc. IEEE/RSJ Int. Conf. Intell. Robot. Syst.,* Edmonton, Albert, Canada, 2005, pp. 2833-2838.

[8] E. Owen and L. Montano, "A robocentric motion planner for dynamic environments using the velocity space," in *Proc. IEEE/RSJ Int. Conf. Intell. Robot. Syst.,* Beijing, China, 2006, pp. 4368-4374.

[9] D. Wilkie, J. V. D. Berg, and D. Manocha, “Generalized velocity obstacles,” in *Proc. IEEE/RSJ Int. Conf. Intell. Robot. Syst.,* St. Louis, MO, 2009, pp. 5573-5578.

[10] J. D. Jeon, H. W. Yu, and B. H. Lee, “Dynamic obstacle avoidance of a differential drive robot using the velocity obstacles in polar coordinates,” in *Proc. 9th Korea Robot. Soc. Annu. Conf.,* Buyeo, Korea, 2014, pp. 271-274.

[11] Adept MobileRobots Pioneer 3-DX (P3DX). [Online]. Available: http://www.mobilerobots.com/ResearchRobots/PioneerP3DX.aspx

[12] L. Zeng and G. M. Bone, “Collision avoidance for non-holonomic mobile robots among unpredictable dynamic obstacles including humans,” in *Proc. IEEE Conf. Autom. Sci. Eng.,* Toronto, Canada, 2010, pp. 940-947.

[13] Y. Abe and M. Yonshiki, “Collision avoidance method for multiple autonomous mobile agents by implicit cooperation,” in *Proc. IEEE/RSJ Int. Conf. Intell. Robot. Syst.,* Maui, HI, vol. 3, 2001, pp. 1207-1212.

Jae D. Jeon received the B.S. degree in electrical engineering from Seoul National University, Seoul, the Republic of Korea in 2011, where he is currently working toward the Ph.D. degree with the Department of Electrical and Computer Engineering. His current research interests include multi-agent system cooperation, multi-robot formation control, and collision avoidance.

Beom H. Lee received the B.S. degree and M.S. degree in electronics engineering from Seoul National University, Seoul, the Republic of Korea in 1978 and 1980, respectively, and the Ph.D. degree in computer, information, and control engineering from the University of Michigan, Ann Arbor, MI in 1985. He was an Assistant Professor with the School of Electrical Engineering at Purdue University, West Lafayette, IN from 1985 to 1987. He joined Seoul National University in 1987, and is currently a Professor with the Department of Electrical and Computer Engineering. His research interests include multi-agent system coordination, control, and application. Prof. Lee has been a Fellow of the Robotics and Automation Society since 2004.